Finite-size effects in nanocomposite thin films and fibers

D. R. Stevens, E. W. Skau, L. N. Downen, M. P. Roman, and L. I. Clarke[*]

Department of Physics, NC State University, Raleigh, North Carolina 27695-8202, USA

Monte Carlo simulations of finite-size effects for continuum percolation in three-dimensional, rectangular sample spaces filled with spherical particles were performed. For samples with any dimension less than 10–20 times the particle diameter, finite-size effects were observed. For thin films in the finite-size regime, percolation across the thin direction of the film gave critical volume fraction (p_c) values that differed from those along the plane of the film. Simulations perpendicular to the film for very thin samples resulted in p_c values lower than the classical limit of $\sim$29% (for spheres in a three-dimensional matrix) which increased with film thickness. For percolation along thin films, while holding film thickness constant, p_c increased with increasing sample size, which is a modification of the finite-sized scaling effect for cubic samples. For samples with a large aspect ratio (fibers) and a finite-sized cross-sectional area, the critical volume fraction increased with sample length, as the sample became quasi-one-dimensional. The results are discussed in the context of adding volume along or perpendicular to the percolation direction. From an experimental perspective, these findings indicate that sample shape, as well as relative size, influences percolation in the finite-size regime.

I. INTRODUCTION

Nanocomposite materials (a matrix doped with nanometer-sized particles) rely on the formation of a network of particles which spans the sample to enhance the properties of the matrix. This first occurs at a critical filling level or percolation threshold (p_c), which is dependent upon many characteristics of the composite, including the sample dimensionality [1]. As fabrication of, and interest in large aspect ratio particles has increased in recent years, the effects of *particle* shape, size, and alignment have been a focus of experimental and computational studies of percolation [2–5]. However increasingly, rather than utilizing bulk sample geometries, composites are being formed into more complex morphologies, such as coatings, thin films, and fibers, where the size of sample features may approach that of the particle, the *sample* shape is anisotropic, and void space may exist within the sample. In these constrained geometries, the sample shape will affect the observed critical filling level, and critical filling may occur at different values along different axes of the sample. For instance, Fu *et al.* recently reported changes in p_c for thin films as film thickness approached the length of the carbon nanotube dopant [6]. As well, we have experimentally observed similar effects as a function of sample size in fibrous mats doped with carbon nanotubes [7]. More broadly, percolation in a confined geometry is generally important for particle-doped nanofibers, such as those fabricated by electrospinning [8] where the fiber diameter may approach the size of at least one dimension of the particle. The underlying issues of percolation within these confined spaces and anisotropic finite-sized samples have not previously been well studied, particularly with an eye toward understanding current, technologically important experimental geometries, such as thin films and nanofibers. In fact, many applications for nanocomposites involve thin films or coatings of either a continuous (filmlike) or fibrous morphology.

In this report, we discuss computational results on finite-size effects along long fibers and within thin films, where percolation is measured either along or perpendicular to the thin film. Here we focus on spherical particles; however, these effects are also significant for technologically important large aspect ratio particles, and scale based upon the longest particle dimension; that is, in order to avoid finite-size effects a sample size of many times the longest particle dimension is required, as will be discussed in a future report [7]. Previously, our group [9] as well as others [10], have addressed the effect of void space within complex morphologies.

II. COMPUTATIONAL DETAILS

Three-dimensional (3D) continuum Monte Carlo simulations were performed as reported earlier [9]. Sample spaces were doped with completely penetrable (soft core) spheres of a fixed size. For a given sample space and doping level, 1000 or more realizations were generated and tested for percolation, resulting in a percolation probability for each case. Percolation tests were carried out using a "tree-burning" algorithm [11]. The critical volume fraction was defined as the filling level at which the percolation probability was 50%, as determined by fitting the probability versus volume fraction curve with the equation $P = 0.5 + 0.5 \, \text{erf}[(p - p_c)/\Delta]$ where P is the percolation probability, erf the error function, p the volume fraction, and Δ reflects the width of the transition region [12]. In our terminology p_c is a size- and shape-dependent parameter due to finite-size effects; p_c^∞ is the infinite limit of this value or the usual critical volume fraction. Volume fractions were determined from either $1 - p = (1 - v/V)^N$ or the infinite limit form of this equation $p = 1 - \exp(-vN/V)$ where N is the number of particles, v is the particle volume, and V is the space available for filling, that is, for placement of the center point of the filling particle [13], modified as follows to account for particle volume residing outside the sample space. Assuming a uniform distribution of particles throughout the sample, the probability of a particle touching $n = 0$, 1, or 2 sides of the sample space, the expected

* liclarke@ncsu.edu

protruding volume in each case, and thus the expected enclosed volume $\langle v_n \rangle$ were calculated. The volume fraction is then $p = 1 - \exp[-N(vP_0 + \langle v_1 \rangle P_1 + \langle v_2 \rangle P_2 + \langle v_3 \rangle P_3)/V]$ [14]. The error in p_c is the standard deviation ($\sigma = \Delta/\sqrt{2}$ as the error function is the integral of a Gaussian distribution) calculated from the fit of the probability versus volume fraction data. For very small samples, we directly calculated p by checking a few million points within the sample (either randomly or by imposing a fine grid) and determining if each fell within a sphere [15]. For the largest sample sizes, instead of traditional Monte Carlo, a series of correlated tree-burning tests were performed. A very low doping level was generated and the absence of percolation confirmed. This same particle placement was retained and additional particles were added, iterating until percolation was achieved. The critical particle number was recorded, generating a p_c value for this realization, using the above formulaic approach. The process was repeated 1000 times and a percolation probability versus volume fraction curve was generated by numerically integrating the data, and then fit as described above. In this approach, there is less statistical sampling away from p_c; however, for 35 test cases of various shapes, we found good agreement with traditional Monte Carlo, providing the sample is sufficiently large. A similar approach has been previously reported [16].

III. RESULTS AND DISCUSSION

A. Finite-size effects in cubes

Finite sample size effects have previously been studied primarily in cubic or square systems. In these cases, as the sample size increases, p_c approaches an asymptotic value from above, $p_c - p_c^\infty \sim L^{-1/\nu}$ with L the sample length and ν the scaling exponent [1]. Figure 1 shows the probability curves for cubic samples of varying size. Following the intersection with the dashed line (50%) reveals that the critical volume threshold decreases as the sample size increases. In addition, the transition becomes sharper, also as expected from classical theory where $\Delta \sim L^{-1/\nu}$ [1,12]. Scaling Δ values (for 13 cubes with $L = 20$–70) resulted in $\nu = 0.91 \pm 0.02$ consistent with a previous report of $\nu = 0.89 \pm 0.01$ for cubes with $L = 16$–80 ($p_c^\infty = 0.2895 \pm 0.0005$) [12]. For smaller cubes ($L = 2, 5, 10,$ and 15), Δ was smaller than expected from this scaling law with the deviation increasing with decreasing size. Utilizing this Δ value to scale the p_c data resulted in $p_c = 0.2887 \pm 0.0001$ which is slightly lower than the previous finite-size scaling value and a very accurate recent value of $p_c = 0.289573 \pm 0.000002$ [17]. This slight deviation may be due to our handling of protruding volume. Without the protruding volume adjustment, which is a small correction at large sample size, but significant for small samples, our results yield $\nu = 0.90 \pm 0.02$ with $p_c^\infty = 0.2891 \pm 0.0002$ which is fully consistent with previous finite-size scaling studies.

One interpretation of this classical result is that for similar particle and sample size, generating a single sample-spanning path requires few particles but a large fraction of the sample volume. For a cubic sample, as the sample gets larger, the length to be spanned (and thus the number of particles needed) increases, however, the overall volume rises more rapidly, so a smaller fraction of the overall sample will be filled at the
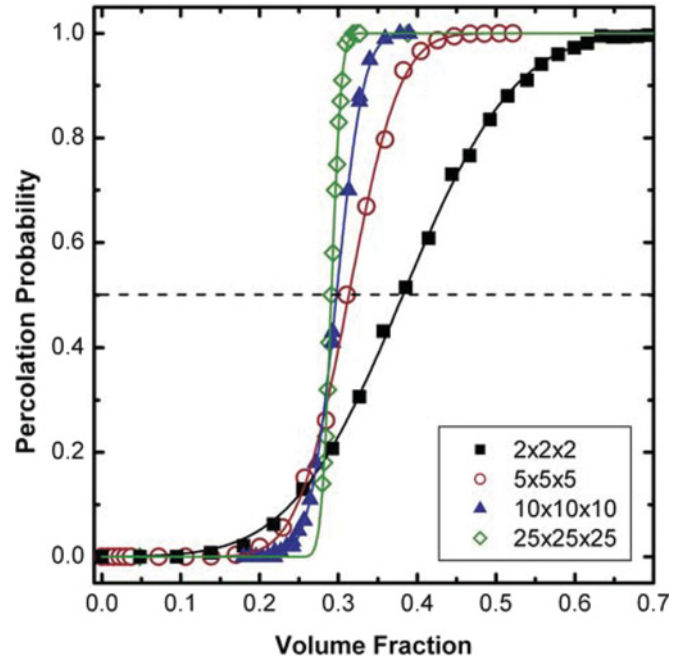

FIG. 1. (Color online) Percolation probability curves for cubic samples doped with spheres. Fit lines are error function. Sample dimensions are relative to sphere diameter. The dashed horizontal line indicates 50% percolation probability.

percolation threshold. The net effect is a decrease in p_c with increasing sample size for small samples.

B. Finite-size effects in fibers

In contrast, for a fiberlike sample where percolation occurs along the long axis, an increase in the fiber length while maintaining cross-sectional area (A) provides only a modest increase in volume. Thus, the length effect dominates and p_c grows with increasing fiber length. This case is presented in Fig. 2 where cubic samples for five different cross-sectional areas were extended in the direction of percolation, resulting in a more fiberlike shape. As the sample lengthens, p_c increases, with the size of the effect the largest for the most confined samples, where particle size is similar to the cross-sectional area of the fiber. For small cross-sectional areas, as the fiber length increases, the samples become quasi-one-dimensional (quasi-1D) and, as a result p_c grows. In the most extreme case ($L = 200$, $A = 1 \times 1$), p_c is 0.960 approaching the true 1D value of 1. As the cross-sectional area increases the effect is lessened. Considering the asymptotic values at large L as the most experimentally accessible, even for a cross-sectional area of 10×10, p_c is noticeably elevated over the usual three-dimensional value. For a sufficiently large cross-sectional area we expect to recover this bulk (3D) value of p_c of ~ 0.29 with no dependence on sample aspect ratio. Samples with a cross-sectional dimension of $50 \times$ and $100 \times$ approach this value ($L = 200$, $A = 50 \times 50$ $p_c = 0.296$; $L = 50$, $A = 100 \times 100$ $p_c = 0.284$) although p_c is still somewhat shape dependent. Scaling using the form $|p_c - p_c^\infty| \sim L^{-1/\nu}$ (where the absolute value is necessary as p_c falls below the infinite limit value) is summarized in the Fig. 2 caption. For large cross-sectional areas, the
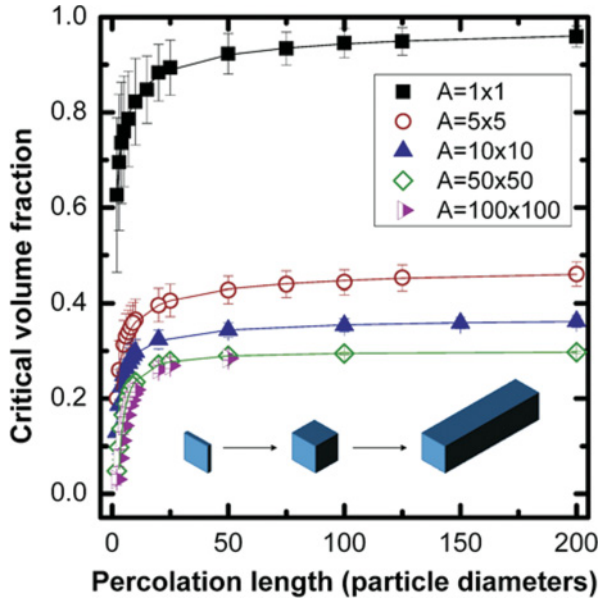
FIG. 2. (Color online) Thin film to cubic to fiberlike transition for five different cross-sectional areas. Sample dimensions are relative to sphere diameter and percolation is tested for along L the percolation length. A is the cross-sectional area perpendicular to L. Fit lines are from the standard p_c finite-sized scaling form (taking the absolute value of the left-hand side) with p_c^∞ and ν values as follows: $A = 1 \times 1$, 1.003 ± 0.004, 2.11 ± 0.08; $A = 5 \times 5$, 0.495 ± 0.003, 2.23 ± 0.08; $A = 10 \times 10$, 0.376 ± 0.001, 1.72 ± 0.05; $A = 50 \times 50$, 0.2995 ± 0.0006, 0.88 ± 0.05; $A = 100 \times 100$, 0.299 ± 0.003, 0.94 ± 0.05. As expected, the smallest L values do not scale; more low L values had to be excluded as cross-sectional area increased. An elevated ν indicates a slower approach to the infinite value as L is increased. We also scaled samples with the same aspect ratio (AR) versus L. For a small number of samples with AR $= 2$, $p_c^\infty = 0.289$ and $\nu = 0.88$; ν increased as AR varied from 1 (e.g., AR $= 1/5$, $\nu = 2.2$; AR $= 15$, $\nu = 1.1$). Again, small L values do not scale.

scaling exponent (ν) and p_c values approach those in 3D. For anisotropic samples (either thin filmlike or fiberlike), ν is elevated, indicating a slower approach of p_c to the infinite value or equivalently, the need for a larger sample in order to avoid finite-size effects.

C. Finite-size effects in thin films

Interestingly, a second effect is noticeable in Fig. 2 for sample aspect ratios less than one. In this region, where the length of the sample is less than $\sqrt{A}$, for large sample sizes, p_c is lower than the three-dimensional value of $\sim$0.29, normally considered the lower limit. In this case, the sample length along which percolation is measured is small (a few particle diameters), while the cross-sectional area can be relatively large, thus very little of the volume must be filled in order to span this short distance. Similar results along and across rectangular samples have been observed in two-dimensional (2D) lattice percolation simulations [18–20]. This result led us to examine such thin filmlike geometries, where percolation can be experimentally measured along the short "thickness" of the sample, for instance, when the film is placed between
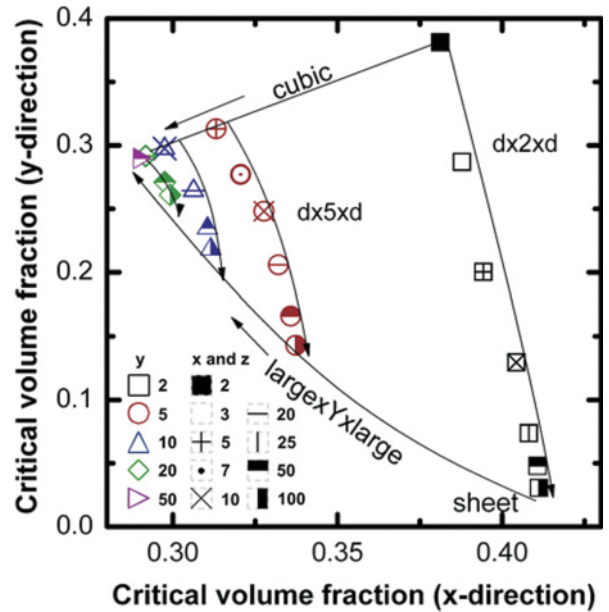

FIG. 3. (Color online) Critical volume fraction in two directions (x and y as indicated above) for cubic to filmlike samples. The x and z dimensions are always the same ($=d$), so percolation occurs perpendicular to or along a filmlike sample. Dimensions are in units of the sphere diameter. Arrows point in the direction of larger samples. For comparison, the values in Fig. 2 are in the y direction.

parallel-plate electrodes, or alternatively along the plane of the film. In fact, for the largest cross-sectional dimensions ($50\times$ and $100\times$) in Fig. 2, the results are almost independent of the cross-sectional area, indicating that these limiting values are applicable for thin films (very large A, with much smaller L). In this case, the primary finite-size effect is a significant decrease in p_c at L values less than $\sim$20$\times$, even though the other sample dimensions are quite large.

The results for thin films (and smaller samples with aspect ratio <1) in comparison with cubes are summarized in Fig. 3. We first discuss percolation along the thin direction, perpendicular to the film (the y axis in Fig. 3). For instance, for a sample thickness of $2\times$ the particle diameter (squares), as the cross-sectional area of the sample increases [e.g., from 2×2 (fully filled) to 100×100 (right-half filled)], p_c along y ($p_{c,y}$) decreases, falling well below the classical limit of $\sim$0.29. We term this result the "thin-wide sample" effect, to distinguish it from the other finite-size effects, namely the "fiber" effect (Fig. 2) and the "classical finite scaling" effect (Fig. 1). This decrease is related to the classical scaling effect, where p_c is driven downward as total volume increases. Here the counteracting effect due to increasing sample length is absent as the sample thickness remains constant. Further increase in the cross-sectional area (and thus the volume), continues to decrease $p_{c,y}$ until the values begin to asymptote at large A (here the x-z plane). As the thin-film samples become thicker [e.g., with a thickness of $5\times$ (circles in Fig. 3)], increasing the cross-sectional area still reduces $p_{c,y}$, but to a lesser extent. As sample size increases, p_c values converge toward the point $p_{c,y} = p_{c,x} \approx 0.29$, exemplified by the $50 \times 50 \times 50$ sample ($p_{c,y} = p_{c,x} = 0.290$). Again, as in the fiber case, the effect is largest for the highest confinement (in

this case, the thinnest sample). Considering the experimentally accessible thin-film case, the large $\times\,Y\,\times$ large line in Fig. 3 follows the transition as the thickness of a thin film (very large A) increases. Again, it is noteworthy that noticeable finite-size effects persist up to thicknesses of $20\times$ the particle diameter.

We can also consider percolation along such a film, which would be important experimentally for applications where transport along (rather than just through) the film was crucial (such as cases where electrodes are attached only to the ends of a conducting composite film). Considering again the $y = 2$ sample sequence (squares in Fig. 3), we now examine $p_{c,x}$ (x axis, Fig. 3). Here, the film thickness (y) is kept constant, while both the percolation direction (x) and z (the orthogonal direction within the film) increase simultaneously. Thus, both the percolation direction and one component of the cross-sectional area (now the y-z plane) increase by the same extent. As the sample size grows [e.g., from $2 \times 2 \times 2$ (fully filled) to $100 \times 2 \times 100$ (right-half filled)] $p_{c,x}$ increases. This is similar to the fiber case (Fig. 2), where the sample becomes quasi-one-dimensional as a cubic sample transitions into a fiber, with an associated increase in p_c. Here, the transition is from a three-dimensional sample to a quasi-two dimensional sheet. As in the fiber case, the increase is larger for more confined (in this case thinner) samples, with the thinnest ($2\times$) sample showing the largest increase. For comparison, a sheet of spheres in a rectangular box, one sphere tall, has a $p_{c,x}$ of at least ~ 0.45 (calculated from the known areal volume fraction in 2D of ~ 0.68 for continuum percolation of circles [21]). This value is similar to the result for a $1\times$ thick sample (not shown), $100 \times 1 \times 100$ where $p_{c,x} = 0.51$. As the sample becomes sufficiently thick, the difference in p_c along x and y decreases, and both approach the 3D value. For comparison, traditional finite scaling for cubic samples is highlighted at the top of Fig. 3.

the "thin-wide sample" (increasing the cross-sectional area only) effect lower p_c as sample volume is increased. In other cases (fibers, or increasing film thickness for thin films when percolating along the thin direction), the effect of increasing the percolation length dominates and p_c grows with size. In the experimentally accessible configurations of long fibers or thin films, p_c will be elevated for fibers with finite cross sections and suppressed for thin films. Both of these observations are consistent with previous experimental work by ourselves [7,22, 23] and others [6] with long aspect ratio particles (rather than the spheres studied in this work), indicating that these effects remain important as particle aspect ratio changes. We will address finite-size effects for large aspect ratio particles in a future work [7]. Very recently a study of anisotropic finite-size effects in a three-dimensional continuum system for a much narrower range of sample shapes (square cross sections only with aspect ratios of 0.125–8.0) than in this work (aspect ratios of 0.02–200) has appeared [24].

We have shown that in the finite-size regime both the sample size and shape affect percolation. In classical finite scaling, where volume is added symmetrically in all three directions to the sample, the critical volume fraction decreases with increasing sample size. Conversely, adding volume only along the percolation direction raises the critical volume fraction (the "fiber" effect). In a thin-film geometry, when percolating along the film, increasing the sample size while holding the thickness constant results in a modified version of "fiber" effect where p_c increases but with a slower rate than in the fiber case. Finally, for percolation along the short distance of the film, increasing sample size, while keeping the percolation distance constant, results in a dramatic decrease in p_c and values that are lower than the usual 3D limit (0.29 for spherical particles). All three of these finite-size effects are the largest at a small sample-to-particle ratio and diminish as this confinement is released until at sufficiently large sample sizes the critical volume is independent of sample shape and size and collapses to the 3D limit.

IV. CONCLUSIONS

Summarizing all the results in this work, in the finite-size regime increasing the length of the percolation direction tends to increase p_c, whereas increasing the cross-sectional area perpendicular to percolation drives down the value of p_c. In a given experimental configuration, one of these effects will dominate, leading to either an increase or decrease in p_c with sample size *dependent upon sample geometry*. For instance, both "classical finite scaling" (increasingly larger cubes) and

[1] D. Stauffer and A. Aharony, *Introduction to Percolation Theory* (Taylor & Francis, Philadelphia, 1994).

[2] S. H. Munson-McGee, Phys. Rev. B **43**, 3331 (1991).

[3] A. Celzard, E. McRae, C. Deleuze, M. Dufort, G. Furdin, and J. F. Mareche, Phys. Rev. B **53**, 6209 (1996).

[4] S. I. White, B. A. DiDonna, M. F. Mu, T. C. Lubensky, and K. I. Winey, Phys. Rev. B **79**, 024301 (2009).

[5] J. T. Li and S. L. Zhang, Phys. Rev. E **80**, 040104 (2009).

[6] M. Fu, Y. Yu, J. J. Xie, L. P. Wang, M. Y. Fan, S. L. Jiang, and Y. K. Zeng, Appl. Phys. Lett. **94**, 12904 (2009).

[7] D. R. Stevens, E. W. Skau, T. J. Hoffman, M. P. Roman, L. N. Downen, W. A. Roberts, R. E. Gorga, and L. I. Clarke (in preparation).

[8] K. M. Sawicka and P. Gouma, J. Nanopart. Res. **8**, 769 (2006).

[9] D. R. Stevens, L. N. Downen, and L. I. Clarke, Phys. Rev. B **78**, 235425 (2008).

[10] N. Johner, C. Grimaldi, T. Maeder, and P. Ryser, Phys. Rev. E **79**, 020104 (2009).

[11] Y. B. Yi and A. M. Sastry, Phys. Rev. E **66**, 066130 (2002).

[12] M. D. Rintoul and S. Torquato, J. Phys. A **30**, L585 (1997).

[13] I. Balberg, Phys. Rev. B **33**, 3618 (1986).

[14] R. Consiglio, D. R. Baker, G. Paul, and H. E. Stanley, Physica A **319**, 49 (2003).

[15] J. Quintanilla and S. Torquato, J. Chem. Phys. **106**, 2741 (1997).

[16] M. Foygel, R. D. Morris, D. Anez, S. French, and V. L. Sobolev, Phys. Rev. B **71**, 104201 (2005).

[17] C. D. Lorenz and R. M. Ziff, J. Chem. Phys. **114**, 3659 (2001).

[18] E. Z. Meilikhov, Phys. Lett. A **346**, 193 (2005).

[19] T. Kiefer, G. Villanueva, and J. Brugger, Phys. Rev. E **80**, 21104 (2009).

[20] M. Masihi, P. R. King, and P. Nurafza, Phys. Rev. E **74**, 042102 (2006).

[21] J. Quintanilla, S. Torquato, and R. M. Ziff, J. Phys. A **33**, L399 (2000).

[22] S. D. McCullen, D. R. Stevens, W. A. Roberts, S. S. Ojha, L. I. Clarke, and R. E. Gorga, Macromolecules **40**, 997 (2007).

[23] S. S. Ojha, D. R. Stevens, K. Stano, T. Hoffman, L. I. Clarke, and R. E. Gorga, Macromolecules **41**, 2509 (2008).

[24] S. Sadeghnejad, M. Masihi, P. R. King, A. Shojaei, and M. Pishvaei, Phys. Rev. E **81**, 061119 (2010).